International Journal of Engineering Applied Sciences and Technology, 2021
Vol. 5, Issue 9, ISSN No. 2455-2143, Pages 17-26
Published Online January 2021 in IJEAST (http://www.ijeast.com)

LEARNING SOFT ROBOT AND SOFT ACTUATOR DYNAMICS USING DEEP NEURAL NETWORK

Hari Prakash Thanabalan
School of Engineering and Materials Science
Queen Mary University of London, England, United Kingdom

***Abstract*— Inspired by living organisms and being the forefront of robotics evolution, the research in soft robotics has been growing exponentially. Due to the flexibility of these robots that is made from soft materials such as silicone or even a fabric allows them to manoeuvre on secluded environments through crevice openings which bring many advantages comparing to the rigid-component robots which proves much more delicate interaction with humans and environments. In this paper, modelling of the soft robot using finite element modelling will be discussed in conjunction with deep neural network for the bending and control of the end effector.**

Keywords — **soft robot, soft actuator, finite element modelling, deep neural network**

I. INTRODUCTION

The research on soft robotics has been growing in the recent decade and has been the forefront of robotics evolution. Being inspired by nature, the goal of a soft robot is replicate and understand natures competency in terms of locomotion and grasping. Taking inspiration from natural manipulators such as elephant's trunk (Hannan & Walker, 2003), squid's tentacles (Ranzani, et al., 2015), octopus' arms (Sareh, et al., 2014), snakes (Ahmed & Billah, 2015) and even plants (Putzu, et al., 2018). Soft robots are operated via soft actuators such as electrically, magnetically, thermally, photo, pressure and explosively responsive (El-Atab, et al., 2020). Soft robots can manoeuvre in secluded environment crevice openings due to their compliant structure, that are made from soft materials such as silicone rubber or even fabric. Soft robots embed safety at the material level which provide delicate interaction with humans and the environment. Having monolithic soft bodies, the requirement for assembling a soft robot is minimal and made of low-cost materials further cuts down the manufacturing cost. Previous studies have shown that soft robots have advantages over their traditional rigid counterpart. Applications of soft robotics can be seen in the medical community where soft robots are using in minimal invasive surgery (Ranzani, et al., 2015), cardiac surgery (Roche, et al., 2017), and compliant palpation of soft tissue during medical diagnosis (Putzu, et al., 2018). Soft robots are also used for underwater (Shintake, et al., 2018) and unstructured terrain exploration (Coad, et al., 2020). However, comparing with a rigid robot, modelling a soft robot can be challenging due to their complex dynamics and non-linearity. In this paper, introduces soft robotic arm, controlled pneumatically, where the 3D modelling was done using Finite Element Modelling (FEM) where FEM is used to model structures that involves many nonlinearities such as geometrical, material and contact nonlinearities (Tawk & Alici, 2020) and in conjunction with Deep Neural Networks (DNNs) for the bending and control of the end effector to allow the algorithm to learn the trajectory and bending of the soft robot more accurately. The simulation was performed using ANSYS (ANSYS Inc.) and Python Programming was used to model the DNN algorithm.

II. RELATED WORK

According to several paper published previously, there are various methods for the bending and control of the end effector. A paper proposed by (Ataka, et al., 2020) where the model-based kinematics were used to control the robot's tip position and the direction, and the Euler-Bernoulli's theory was used to control the bending segment of the robot for its structural stiffness. Using constant curvature method as a kinematic model proposed by (Mosqueda, et al., 2018) where the model was used to establish a relation between continuum robots and mathematical model. The field of Artificial Intelligence (AI) and Machine Learning (ML) has been growing dramatically in the field of robotics where AI and ML can improve the accuracy and efficiency of a

International Journal of Engineering Applied Sciences and Technology, 2021
Vol. 5, Issue 9, ISSN No. 2455-2143, Pages 17-26
Published Online January 2021 in IJEAST (http://www.ijeast.com)

robot. Paper proposed by (Chin, et al., 2020) where data from the physical environment was gathered using soft sensors and transducing these data into a signal that converts the information. The use of machine learning was then used to decode the signal to mimic the representation of the actual phenomenon. Similarly, (Kovandžić, et al., 2019) where the inverse kinematics of a soft robot was explained using artificial neural network (ANN) given the desired spatial coordinates of the robot as the input and the step motor angular displacement as the output where the neural network was used to estimate the behaviour of the system.

III. MODELLING OF FLEXIBLE LINK MANIPULATORS

Modelling flexible link manipulators could be challenging due to its flexibility. Therefore, several methods have been used to model a flexible link manipulator. Previous studies have implemented the application of Lagrangian technique in conjunction with Assumed Mode Method (AMM) for modelling of flexible link manipulators as proposed by (Khairuddin, 2015). A more conventional method of modelling a flexible link manipulator is by using Piecewise Constant Curvature (PCC) using Denavit-Hartenberg (D-H) method. According to (Runge, et al., 2017) PCC could describe kinematics by circular arcs as described in the Fig.1.

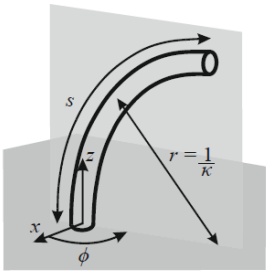

Figure 1: Parameters that describe a circular arc

The parameters that describe the circular arc which consist of curvature (κ), arc length (s) and the plane angle ($\emptyset$) can be written as shown in Eq.1 and Eq.2 (Runge, et al., 2017) and r is denoted as the radius:

$$\theta = \kappa s \; (s \in [0 \; l]) \qquad (1)$$

$$\kappa = 1/r \qquad (2)$$

The augmented D-H matrix could be written in a homogenous transformation matrix shown in Eq.3 (Runge, et al., 2017):

$$A = \begin{bmatrix} cos^2\emptyset(\cos\kappa s - 1) + 1 & sin\emptyset cos\emptyset(\cos\kappa s - 1) & cos\emptyset \sin\kappa s & \frac{cos\emptyset(1-\cos\kappa s)}{\kappa} \\ sin\emptyset cos\emptyset(\cos\kappa s - 1) & cos^2\emptyset(1 - \cos\kappa s) + \cos\kappa s & sin\emptyset \sin\kappa s & \frac{sin\emptyset(1-\cos\kappa s)}{\kappa} \\ -cos\emptyset \sin\kappa s & -sin\emptyset \sin\kappa s & \cos\kappa s & \frac{\sin\kappa s}{\kappa} \\ 0 & 0 & 0 & 1 \end{bmatrix} \qquad (3)$$

IV. MODELLING OF FLEXIBLE LINK MANIPULATOR USING DEEP NEURAL NETWORK

Implementation of deep neural network was deployed in conjunction with the flexible link manipulator. Crucial hyperparameters such as learning rate, α and the regularizer, λ was set to 0.001. Regularization was added into the equation to make minor adjustments to the learning algorithm to allow the model to generalize well to prevent overfitting. Regularization term is added to the cost function equation which results in Eq. 4 (Sham, 2020):

$$J(\theta) = -\frac{1}{m}\left(\sum_{i=1}^{m}\sum_{k=1}^{K} y_k^{(i)} \log\left(h_\theta(x^i)\right)_k + \left(1 - y_k^{(i)}\right)\log(1 - (h_\theta(x^i))_k\right) + \frac{\lambda}{2m}\sum_{l=1}^{L-1}\sum_{i=1}^{s_l}\sum_{j=1}^{s_{l+1}}\left(\theta_{ji}^{(l)}\right)^2 \qquad (4)$$

Possible trajectories and the algorithm's learning performance are plotted using Python programming.

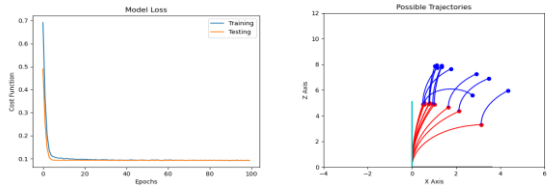

Figure 2: (Left) The plot of algorithm's learning performance over time (Right) Possible trajectories of 2 link flexible manipulator

International Journal of Engineering Applied Sciences and Technology, 2021
Vol. 5, Issue 9, ISSN No. 2455-2143, Pages 17-26
Published Online January 2021 in IJEAST (http://www.ijeast.com)

V. MODELLING SOFT FLEXIBLE MANIPULATORS USING FINITE ELEMENT ANALYSIS

The effective way to model and simulate soft bodies robots is FEM where it has the potential of handling non-linearities and great deformation of the material (Xavier, et al., 2020). For this paper, Ecoflex 00-50 was used. The material property of Ecoflex is softer in comparison with other types of elastomers where lower pressure is required for bending and extension of the soft robot (Xavier, et al., 2020).

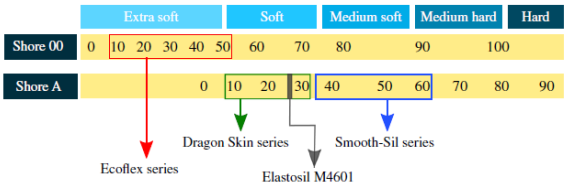

Figure 3: Shore hardness of elastomers used in soft robotics

A. Material Hyperelastic Models

There are several hyperelastic models used in modelling soft robotics - Mooney-Rivlin, Neo-Hookean, Yeoh and Ogden (Xavier, et al., 2020). In this paper, Yeoh model was used due to great elastic behaviour with high success over large range of stress and this model also predicts the stress-strain behaviour for different types for deformation.

a. Neo-Hookean Model
Simplest model which consist of one material constant and could be used for models that has small strain (< 50%)

$$W = C_1(I_1 - 3) = \frac{\mu}{2}(I_1 - 3) \qquad (5)$$

b. Mooney-Rivlin Model
A widely used hyperelastic material which is suitable for models that strains does not exceed over 200%.

$$W = \sum_{i=0,j=0}^{n} C_{ij}(I_1 - 3)^i(I_2 - 3)^j \quad (6)$$

c. Ogden Model
Ogden model is one of the commonly used phenomenological model to allow model deformation that exceed 400% (Ghamsari, 2018).

$$W = \sum_{i=1}^{N} \frac{\mu_i}{\alpha_i}(\lambda_1^{\alpha_i} + \lambda_2^{\alpha_i} + \lambda_3^{\alpha_i} - 3) \quad (7)$$

d. Yeoh Model
One of the most used models for large strain problems that can exceed 400% (Elsayed, et al., 2014)

$$W = \sum_{i=1}^{N} C_{i0}(\bar{I}_1 - 3)^i \qquad (8)$$

B. Modelling Soft Robot using ANSYS

The FE simulation was performed using ANSYS where there are there three basic ANSYS software – Workbench, SpaceClaim and Mechanical. ANSYS Workbench, where material defining takes place and "Static Structural Analysis" was used. Under "Engineering Data", the type of hyperelastic material and model was defined. Yeoh 3rd order was used, and the material constants are defined as shown in Table.1.

Hyperelastic Material Model	Material Constant	Value	Unit
Yeoh (3rd Order)	C10	0.019	MPa
	C20	0.0009	MPa
	C30	$-4.75x10^{-6}$	MPa
	Incompressibility Parameter D1	0	MPa^{-1}
	Incompressibility Parameter D2	0	MPa^{-1}
	Incompressibility Parameter D3	0	MPa^{-1}

Table 1: Ecoflex 00-50 Hyperelastic Material Constant

ANSYS SpaceClaim is a computer aided design (CAD) tool that is used to model desired geometry where. In this paper, single and double chamber actuator are designed where each chamber consists of 3 internal hollow chambers.

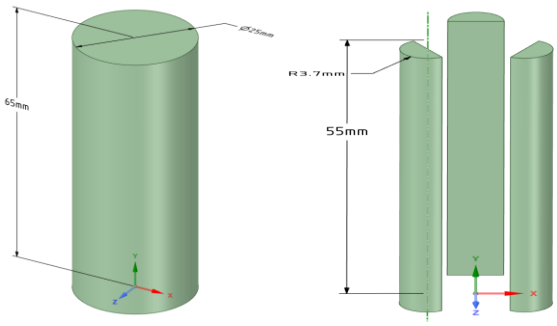

Figure 4: (Left) Dimensions for main chamber and (Right) Dimensions for hollow internal chambers

International Journal of Engineering Applied Sciences and Technology, 2021
Vol. 5, Issue 9, ISSN No. 2455-2143, Pages 17-26
Published Online January 2021 in IJEAST (http://www.ijeast.com)

In ANSYS Mechanical, simulation of the soft robot was performed where it is a dynamic environment that comes with many ranges of analysis tool from preparing geometry for analysis to linking it with additional physics for even better accuracy that could simulate the real environment. Crucial settings were done in ANSYS Mechanical:

- Meshing
  A Quadratic Element Order was used for the mesh settings to retain midside nodes on the model. Given the nature of the model can undergo large deformation, a very fine mesh is not recommended. A mesh size between 0.001 and 0.005m could be used as a starting point.

- Contact
  "Symmetric Behaviour" was used where this results in more accurate and realistic behaviour. "Augmented Lagrange" was a recommended formulation for frictional and frictionless contact where it adds additional control that automatically minimizes penetration.

- Joint
  This setting is used for $n+1$ number of actuators. "Body-to-body" connection type was used to link two actuators and "Fixed" type was selected.

- Analysis Settings
  "Large Deflection" was turned on to perform simulation by considering the large deformation that occurs in soft bodied robots. "Auto Time Stepping" was turned on and the model was solved using time. A good starting point for the initial and the minimum time step are between 0.001 to 0.01 and the maximum time step is between of 0.01 to 0.05

- Boundary Conditions
  "Fixed Support" and "Pressure" are the two main physics tool that was applied. Fixed Support was applied at the bottom of the model to where this lowers the degree of freedom (DoF) of the applied area. Pressure was varied from 20kPa to 28kPa.

VI. RESULTS AND DISCUSSION

Pressure was applied individually in each of the internal chambers where the pressure value ranges from 20kPa to 28kPa and the volume expansion of the internal chamber due to the pressure applied was observed. For 2-chamber actuators, pressure was applied simultaneously on each chamber. The size of the internal chamber ballooning is directly proportional to the applied pressure and the bending angle of the actuator. Fig.5 shows the applied pressure in each internal chamber and Fig.6 shows bending of the actuator when different pressure is applied. Fig.8 shows the bending of 2-chamber actuator with different pressure applied to each internal chamber. The key factor that influences the bending of the actuator is the length of the internal chamber where shorter internal chamber height can drastically affect the bending of the actuator. Fig.9 shows the bending of the soft actuator with respect to different lengths of the internal chamber. Stated in (Elsayed, et al., 2014), the ratio internal chambers and the main chambers should be more than 80% and can be computed using Eq. 9:

$$Ratio\ (\%) = \frac{Internal\ chamber\ height}{Main\ chamber\ height} x100\% \quad (9)$$

The FEM results in terms of displacement, m, applied pressure, kPa and bending angle, °, are extracted as shown in Fig10 and Fig. 11. These results are then used as a training dataset for the neural network algorithm. Fig.10 shows the 1000 data points extracted from ANSYS. Hyperparameters for the neural network are the learning rate α, the use of regularizer λ, number of epochs and number of nodes in the hidden layer were taken into consideration where α = 0.001, λ = 0.001 and the number of epochs is set to 500. The number of epochs was solely based on trial and error method where there are no specific rules that shows the common number of epochs that can be used. There are several sizes of data split which are 80% training data, 10 % test data and 10% validation data (80-10-10), 70% training data, 15 % test data and 15% validation data (70-15-15) and 60% training data, 20 % test data and 20% validation data (60-20-20). For this paper, 80-10-10 and 60-20-20 data split were used. The use of 2 different types of data size was to compare the performance of the neural network where the results are compared in terms of Mean Squared Error (MSE) and Mean Absolute Error (MAE).

International Journal of Engineering Applied Sciences and Technology, 2021
Vol. 5, Issue 9, ISSN No. 2455-2143, Pages 17-26
Published Online January 2021 in IJEAST (http://www.ijeast.com)

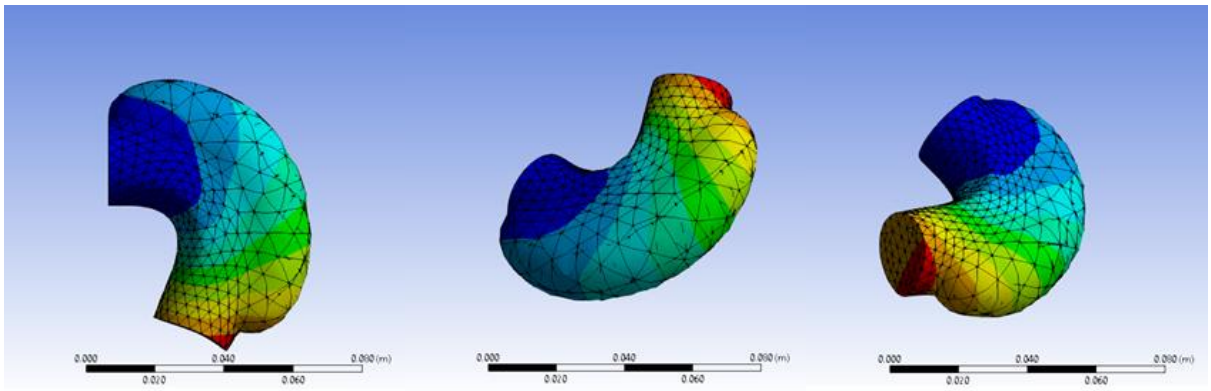

Figure 5: (Left)28kPa pressure applied in internal chamber 1 (Middle) 28kPa pressure applied in internal chamber 2 (Right) 28kPa pressure applied in internal chamber 3

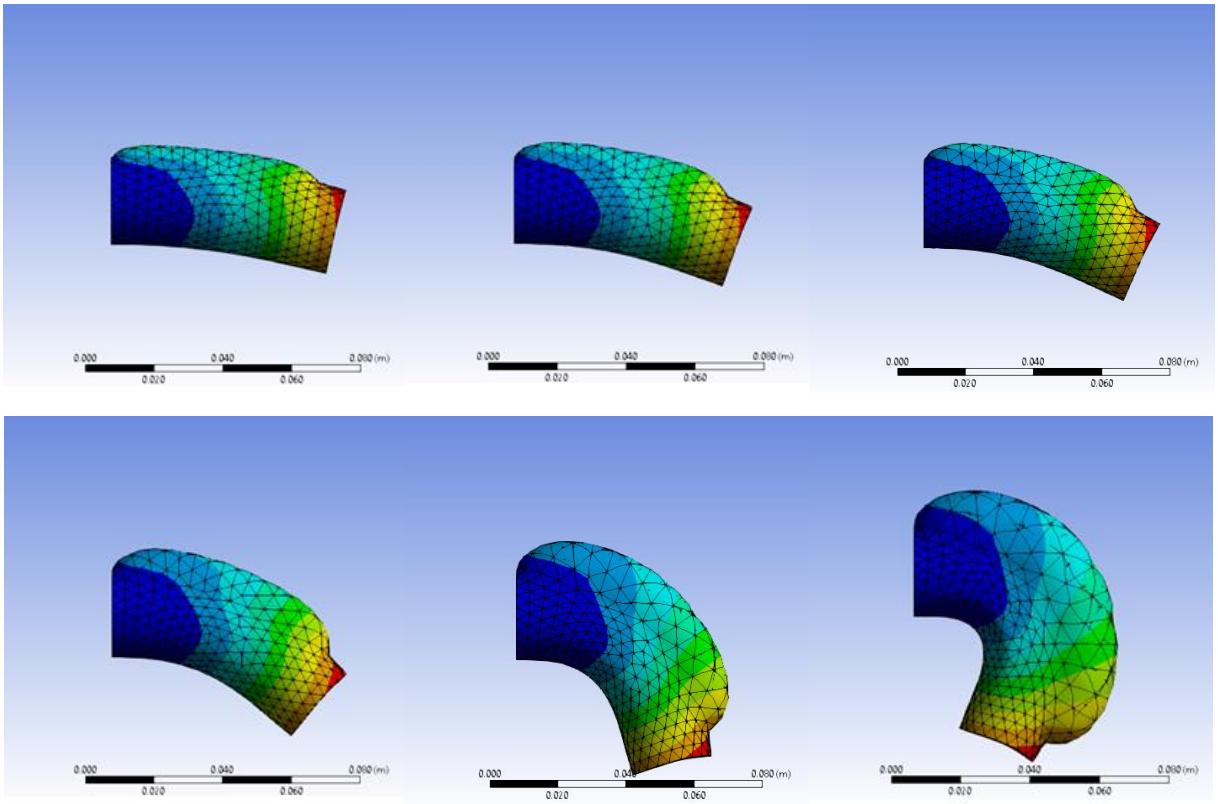

Figure 6: (Top Left) Bending of soft robot at 20kPa pressure (Top Middle) Bending of soft robot at 22kPa pressure (Top Right) Bending of soft robot at 23kPa pressure (Bottom Left) Bending of soft robot at 25kPa pressure (Bottom Middle) Bending of soft robot at 27kPa pressure (Bottom Right) Bending of soft robot at 28kPa pressure

International Journal of Engineering Applied Sciences and Technology, 2021
Vol. 5, Issue 9, ISSN No. 2455-2143, Pages 17-26
Published Online January 2021 in IJEAST (http://www.ijeast.com)

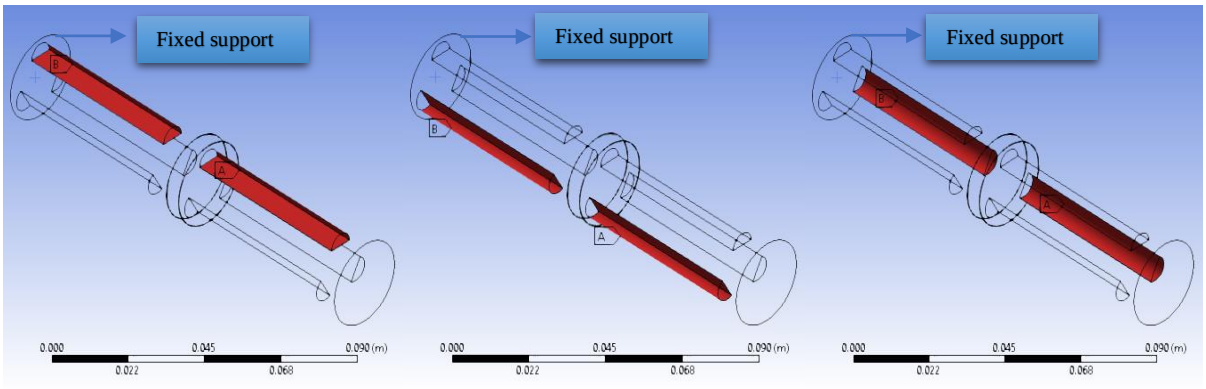

Figure 7: (From the fixed support) (Left) Internal Chamber 1 with Internal Chamber 4 (Middle) Internal Chamber 2 with Internal Chamber 5 (Right) Internal Chamber 3 with Internal Chamber 6

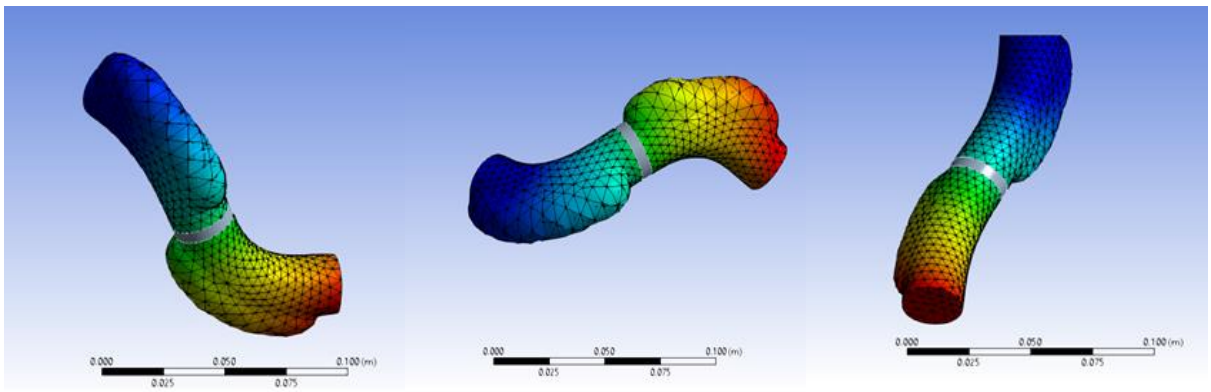

Figure 8: (Left) 28kPa pressure applied in both internal chamber 1 and internal chamber 5 (Middle) 28kPa pressure applied in both internal chamber 2 and internal chamber 4 (Right) 28kPa pressure applied in internal chamber 3 and 25kPa applied in internal chamber 5

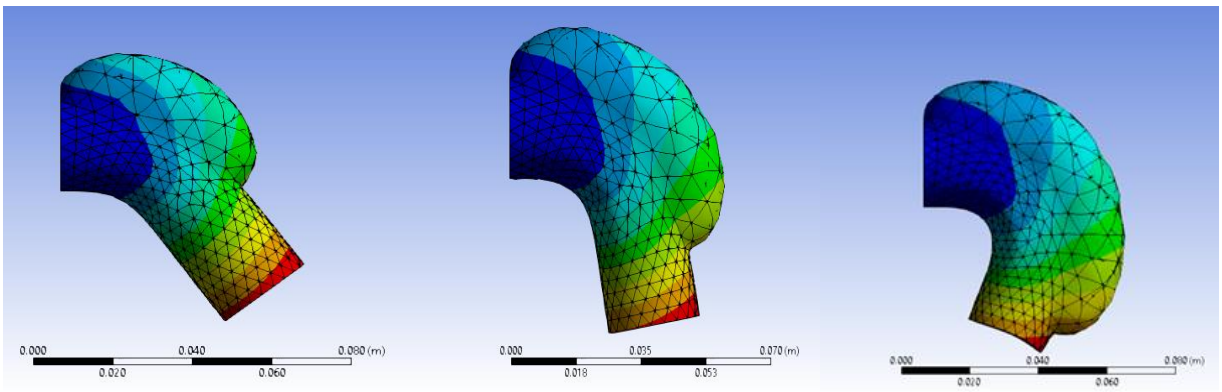

Figure 9: (Left) Bending of the soft robot where the ratio of the length is at 54% (Middle) Bending of the soft robot where the ratio of the length is at 69% (Right) Bending of the soft robot where the ratio of the length is at 85%

International Journal of Engineering Applied Sciences and Technology, 2021
Vol. 5, Issue 9, ISSN No. 2455-2143, Pages 17-26
Published Online January 2021 in IJEAST (http://www.ijeast.com)

	Time [s]	Minimum [m]	Maximum [m]	Average [m]
1	1.e-003	6.5001e-002	6.5001e-002	6.5001e-002
2	2.e-003	6.5001e-002	6.5001e-002	6.5001e-002
3	3.e-003	6.5001e-002	6.5001e-002	6.5001e-002
4	4.e-003	6.5001e-002	6.5001e-002	6.5001e-002
5	5.e-003	6.5001e-002	6.5001e-002	6.5001e-002
6	6.e-003	6.5001e-002	6.5001e-002	6.5001e-002
7	7.e-003	6.5001e-002	6.5001e-002	6.5001e-002
8	8.e-003	6.5001e-002	6.5001e-002	6.5001e-002
9	9.e-003	6.5001e-002	6.5001e-002	6.5001e-002
10	1.e-002	6.5001e-002	6.5001e-002	6.5001e-002
11	1.1e-002	6.5001e-002	6.5001e-002	6.5001e-002
12	1.2e-002	6.5002e-002	6.5002e-002	6.5002e-002

	Time [s]	Minimum [m]	Maximum [m]	Average [m]
989	0.989	3.4159e-002	3.4159e-002	3.4159e-002
990	0.99	3.3459e-002	3.3459e-002	3.3459e-002
991	0.991	3.2749e-002	3.2749e-002	3.2749e-002
992	0.992	3.2045e-002	3.2045e-002	3.2045e-002
993	0.993	3.1313e-002	3.1313e-002	3.1313e-002
994	0.994	3.0563e-002	3.0563e-002	3.0563e-002
995	0.995	2.9784e-002	2.9784e-002	2.9784e-002
996	0.996	2.8984e-002	2.8984e-002	2.8984e-002
997	0.997	2.8174e-002	2.8174e-002	2.8174e-002
998	0.998	2.7352e-002	2.7352e-002	2.7352e-002
999	0.999	2.647e-002	2.647e-002	2.647e-002
1000	1.	2.5581e-002	2.5581e-002	2.5581e-002

Figure 10: (Top) Result of the first 12 end effector position in the X-coordinate (Bottom) Result of the last 12 end effector position in the X-coordinate where the final position of the end effector is 2.5581cm in the X-Axis

	Time [s]	Bending Angle (Z) [°]
1	1.e-003	-4.5023e-004
2	2.e-003	-8.8372e-004
3	3.e-003	-1.3309e-003
4	4.e-003	-1.7918e-003
5	5.e-003	-2.2665e-003
6	6.e-003	-2.755e-003
7	7.e-003	-3.2573e-003
8	8.e-003	-3.7735e-003
9	9.e-003	-4.3036e-003
10	1.e-002	-4.8477e-003
11	1.1e-002	-5.4159e-003
12	1.2e-002	-5.9882e-003

	Time [s]	Bending Angle (Z) [°]
989	0.989	-99.068
990	0.99	-100.27
991	0.991	-101.48
992	0.992	-102.67
993	0.993	-103.91
994	0.994	-105.18
995	0.995	-106.49
996	0.996	-107.84
997	0.997	-109.19
998	0.998	-110.57
999	0.999	-112.05
1000	1.	-113.53

Figure 11: : (Top) Result of the first 12 bending angle (Bottom) Result of the last 12 bending angle where the final angle of curvature is at -113.53°

The number of hidden layers used was 2 and 4 and 8 nodes in each layer are employed to compare the results. A deeper algorithm is not recommended as the data points extracted from ANSYS are 1000 data points. Employing a deeper network, more than 2 hidden layers, will result in overfitting.

	MSE (80-10-10)	**MSE (60-20-20)**
2 Hidden Layers (4 Nodes)	0.0040	0.0052
2 Hidden Layers (8 Nodes)	0.0043	0.0045
	MAE (80-10-10)	**MAE (60-20-20)**
2 Hidden Layers (4 Nodes)	0.0278	0.0324
2 Hidden Layers (8 Nodes)	0.0286	0.0311

Table 2: Comparison between MSE and MAE for 4 nodes and 8 nodes in the hidden layers for 80-10-10 and 60-20-20 data split

The learning curve is a graph that plots the algorithm's learning performance over time. The model can be evaluated based on the training and validation loss after each update during the training of the algorithm and the curve was plotted to measure the model's performance.

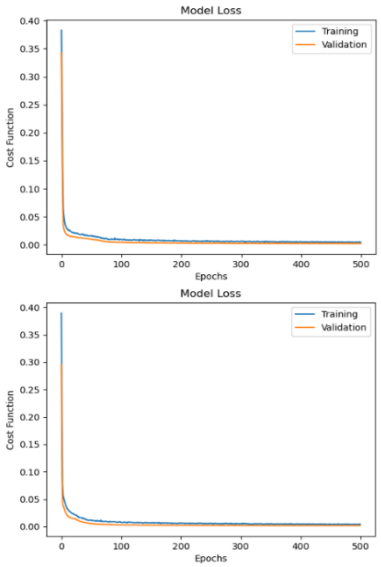

Figure 12: (Top) Learning curve for 2 hidden layers (4 nodes, 80-10-10) (Bottom) Learning curve for 2 hidden layers (8 nodes, 80-10-10)

International Journal of Engineering Applied Sciences and Technology, 2021
Vol. 5, Issue 9, ISSN No. 2455-2143, Pages 17-26
Published Online January 2021 in IJEAST (http://www.ijeast.com)

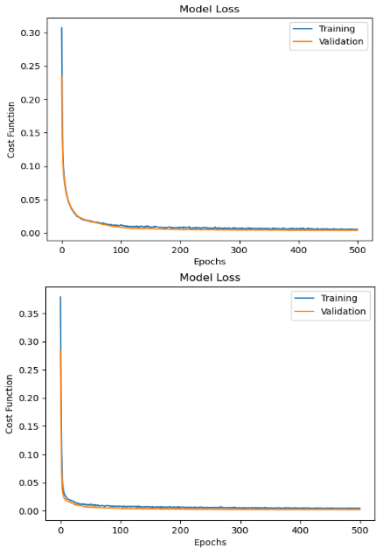

Figure 13: (Top) Learning curve for 2 hidden layers (4 nodes, 60-10-10) (Bottom) Learning curve for 2 hidden layers (8 nodes, 60-10-10)

The indication of an ideal model could be observed when the predicted values are closer to the actual values. The performances on the test in Fig.14-19 show the comparison between the actual and predicted values which are relatively close to each other. This can be concluded that the errors obtained are relatively small which proves to be an ideal model.

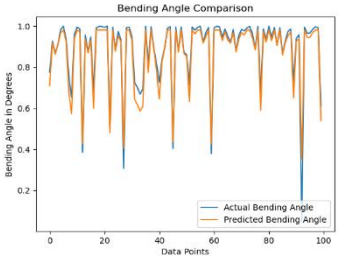

Figure 14: Bending angle comparison between actual value and predicted value

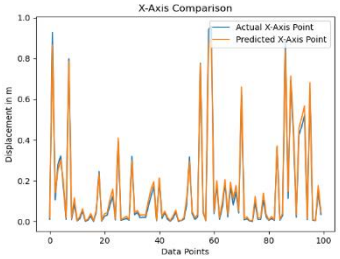

Figure 15: X-Axis coordinate comparison between actual value and predicted value

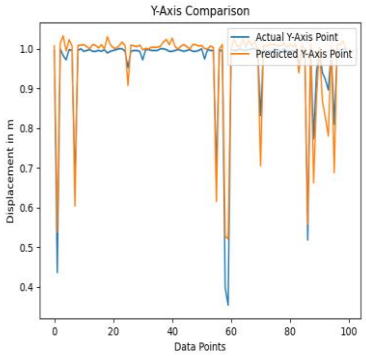

Figure 16: Y-Axis coordinate comparison between actual value and predicted value

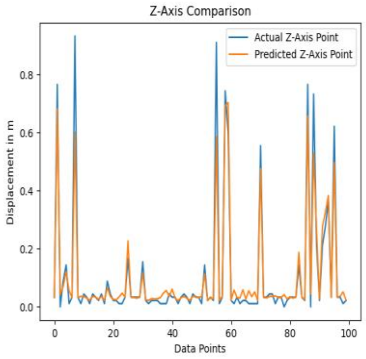

Figure 17: Z-Axis coordinate comparison between actual value and predicted value

VII. CONCLUSION AND FUTURE WORKS

Modelling soft robot using DNNs was proposed effectively where integrating FEM for simulation. Traditional methods such Euler-Bernoulli Beam theory, AMM and D-H method could be used to model a soft robot, in this paper it can be inferred that DNNs proves to be an ideal method to produce highly accurate results. This was proven by observing the results produced by the neural network where the model produces a minute value of error. Prospective studies could focus on modelling actuators more than 2 sections, by improving the existing model. This will then provide a platform where there will be an increase in the section numbers allowing more DoF to achieve a completely soft and flexible link manipulator. This research was conducted by using 1000 data samples which was the maximum number that can be extracted from ANSYS. Further studies could focus more on expanding the data samples.

VIII. REFERENCE

[1] Ahmed, M. & Billah, M. M., 2015. Smart Material-actuated Flexible Tendon-based Snake Robot. *International Journal of Advanced Robotic Systems*, 13(3), p. 10.

[2] Ataka, ,. A. et al., 2020. Model-based pose control of inflatable eversion robot with variable. *IEEE Robotics and Automation Letters*, 5(2), p. 7.

[3] Chin, K., Hellebrekers, T. & Majidi, C., 2020. Machine Learning for Soft Robotic Sensing and Control. *Advanced Intelligent Systems*, 2(6), p. 8.

[4] Coad, M. M. et al., 2020. Vine Robots: Design, Teleoperation, and Deployment for Navigation and Exploration. *IEEE Robotics & Automation Magazine*, 27(3), p. 12.

[5] Ellen T. Roche, Markus A. Horvath, Isaac Wamala, Ali Alazmani, Sang-Eun Song, William Whyte, Zurab Machaidze, Christopher J. Payne, James C. Weaver, Gregory Fishbein, Joseph Kuebler, Nikolay V. Vasilyev, David J. Mooney, Frank A. Pigula and Conor J. Walsh, 2017. Soft Robotic Sleeve Supports Heart Function. *Science Translation Medicine*, 9(373).

[6] Elsayed, Y. et al., 2014. Finite Element Analysis and Design Optimization of a Pneumatically Actuating Silicone Module for Robotic Surgery Applications. *Soft Robotics*, 2(00), p. 8.

[7] Ghamsari, Z. S. N., 2018. *The Introduction and Analysis of a Novel Soft Actuator for a Soft Continuum Robot Arm*, Minnesota: University of Minnesota Duluth.

[8] Hannan, M. W. & Walker, I. D., 2003. Kinematics and the Implementation of an Elephant's Trunk Manipulator and Other Continuum Style Robots. *Journal of Robotic Systems*, 20(2), p. 19.

[9] Khairuddin, M., 2015. Dynamic Modelling of a Flexible Link Manipulator Robot Using AMM. *TELKOMNIKA (Telecommunication Computing Electronics and Control)*, 6(3), p. 7.

[10] Kovandžić, M. et al., 2019. Soft Robot Positioning using Artificial Neural Network. *Automatic Control and Robotics*, 18(1), p. 12.

[11] Nazek El-Atab, Rishabh B. Mishra, Fhad Al-Modaf, Lana Joharji, Aljohara A. Alsharif, Haneen Alamoudi, Marlon Diaz, Nadeem Qaiser, and Muhammad Mustafa Hussain, 2020. Soft Actuators for Soft Robotic Applications: A Review. *Advanced Intelligent Systems*, 2(10), p. 37.

[12] Putzu, F., Abrar, T. & Althoefer, K., 2018. *Plant-Inspired Soft Pneumatic Eversion Robot.* Enschede, 2018 7th IEEE International Conference on Biomedical Robotics and Biomechatronics (Biorob).

[13] Runge, G. B., Wiese, M., Raatz, A. & Günther, L., 2017. *A framework for the kinematic modeling of soft material robots combining finite element analysis and piecewise constant curvature kinematics.* Nagoya, IEEE International Conference on Control, Automation and Robotics.

[14] S. Mosqueda, Y. Moncada, C. Murrugarra and H. Leon-Rodriguez, 2018. *Constant Curvature Kinematic Model Analysis and Experimental Validation for Tendon Driven Continuum Manipulators.* Porto, 15th International Conference on Informatics in Control, Automation and Robotics.

[15] Sareh, S. et al., 2014. Anchoring Like Octopus: Biologically Inspired Soft Artificial Sucker. *Journal of The Royal Society Interface*, 45(135), p. 9.

[16] Sham, S., 2020. *Neural Networks: Cost Function and Backpropagation.* [Online] Available at: https://machinelearningmedium.com/2017/10/03/neural-networks-cost-function-and-back-propagation/ [Accessed 21 November 2020].

[17] Shintake, J., Cacucciolo, V., Shea, H. & Floreano, D., 2018. Soft Biomemetic Fish Robot Made of Dielectric Elastomer Actuators. *Soft Robotics*, 5(4), p. 8.

[18] T. Ranzani, G. Gerboni, M. Cianchetti and A. Menciassi, 2015. A bioinspired soft

manipulator for minimally invasive surgery. *Bioinspiration and Biomimetics,* 10(3), p. 18.

[19] Tawk, C. D. & Alici, G., 2020. Finite Element Modeling in the Design Process of 3D Printed Pneumatic Soft Actuators and Sensors. *Robotics,* 9(3), p. 14.

[20] Xavier, M. S., Fleming, A. J. & Yong, Y. K., 2020. Finite Element Modeling of Soft Fluidic Actuators:Overview and Recent Developments. *Advanced Intelligent Systems,* 2(10), p. 18.